
Every9D-21M: Large-Scale Real-World 9D Canonicalization of Everyday Objects

Leonhard Sommer*
University of Freiburg

Emil Akopyan*
University of Freiburg

Adam Kortylewski
CISPA Helmholtz Center for Information Security

Abstract

Estimating the 9D pose of everyday objects from a single real-world image remains challenging. This is largely due to the lack of large-scale supervision. Most existing datasets either rely heavily on synthetic renderings or provide limited coverage of real-world objects: the largest real-world 9D pose dataset to date contains only 17K annotated objects across 9 categories. We address this gap with Every9D-21M, a dataset of 9D pose annotations for 21.8M real-world images from 109K object-centric videos spanning 700 everyday object categories — two orders of magnitude larger than prior real-world 9D pose benchmarks in both image and category count. To achieve this scale, we leverage object-centric videos by reconstructing object-level point clouds via multi-view geometry and aligning similar instances into a shared canonical coordinate frame. Canonical poses are manually annotated for only a small set of reference objects (fewer than 0.01% of all images) and propagated to the remaining instances via cross-instance alignment. All propagated canonical poses are then verified from multiple viewpoints. We further introduce cross-category orientation rules that induce category-level symmetries, enabling symmetry-aware evaluation. Beyond establishing dedicated training and evaluation splits as a benchmark for 9D pose foundation models, we show that training on Every9D-21M improves performance on ImageNet3D and PASCAL3D+, and generalizes to HANDAL substantially better than training on ImageNet3D. Data and code are available at [GenIntel/Every9D](https://github.com/GenIntel/Every9D).

1 Introduction

Single-image 9D object pose estimation, comprising 3D rotation, 3D translation, and 3D object extent, is fundamental for robotics and AR/VR applications. Recovering these properties from a single RGB image enables spatial reasoning and physical interaction, requiring models to infer consistent object-centric coordinate frames across diverse categories and instances. While recent methods have made progress in category-level 3D pose estimation [45, 67, 57, 19] and full 6D pose estimation [48, 2, 26, 27, 65, 62], achieving reliable 9D pose estimation for general everyday objects remains an open challenge, particularly under unconstrained real-world imaging conditions. Beyond robotics, consistent object canonicalization has become increasingly important for 3D generative modeling. Recent text-to-3D and image-to-3D systems benefit from orientation-aligned training data, as canonical object frames improve controllability and geometric consistency [29, 63, 32]. Similarly, correspondence learning and 3D morphable modeling commonly assume canonicalized objects to ensure stable alignment across instances [34, 10, 5, 16, 37, 9, 66, 46, 43]. These advances highlight the need for scalable real-world canonicalized supervision beyond synthetic data.

*Equal contribution.



Figure 1: **Every9D-21M**. Example canonicalized objects from our dataset. Each object is reconstructed as a 3D Gaussian Splat from an object-centric video in uCO3D. Cross-instance alignment establishes shared canonical coordinate frames, which are subsequently propagated to all video frames, yielding 9D pose annotations for 21.8M real-world images across 700 object categories.

However, most existing large-scale 3D datasets rely on rendered assets [8, 7, 64, 28, 6, 22, 12], which enable scale but are created under synthetic and controlled conditions. Models trained predominantly on such renderings, including the recent OrientAnything models for pose estimation [51, 52], struggle to generalize to real images affected by sensor noise, occlusions, motion blur, and appearance variability. To mitigate this sim-to-real gap, OrientAnything resorts to ImageNet3D [33] for real-world supervision — but image-level 3D pose annotations are prohibitively expensive and fundamentally ambiguous from single views. As a result, existing real-world pose datasets are forced to trade off category diversity against instance scale: the largest 3D pose benchmark, ImageNet3D, covers 200 categories but only 86K images, while the largest 9D pose benchmark, Objectron, covers 4M images but only 9 categories. No existing real-world dataset offers both broad category coverage and large-scale annotation.

To overcome this limitation, we leverage object-centric videos as a scalable source of real-world supervision. For each video, we reconstruct an object-level point cloud via multi-view reconstruction, yielding a geometric representation robust to single-view ambiguities. We then cluster visually similar instances and align their reconstructed point clouds through cross-instance geometric and appearance matching, establishing shared canonical coordinate frames that are propagated from a small set of manually annotated reference objects. Applying this framework to 109K object-centric videos of everyday objects from uCO3D [30] yields 9D pose annotations for 21.8M real-world images across 700 categories. Manual 9D annotation is required for fewer than 0.01% of images, while verification covers every propagated pose from multiple viewpoints. In total, the dataset was produced in 199 hours of human effort — 67 hours of reference annotation and 132 hours of multi-view verification. We refer to this large-scale real-world canonicalization dataset as Every9D-21M.

Our main contributions are the following:

1. **Scalable real-world 9D canonicalization.** We introduce an iterative reference-based canonicalization framework that leverages object-centric videos for multi-view 3D reconstruction and cross-instance alignment. By propagating canonical frames from a small set of annotated reference objects, our approach enables large-scale 9D pose supervision at scale, with every propagated annotation subsequently verified from multiple viewpoints.
2. **Every9D-21M: A large-scale real-world 9D pose dataset.** Using this framework, we canonicalize 109K object-centric videos from uCO3D, providing 9D pose annotations for 21.8 million images across 700 categories. Manual annotation is required for fewer than 0.01% of images, with the entire dataset produced in 199 hours of human effort. Every9D-21M is two orders of magnitude larger than prior real-world 9D pose benchmarks in both image and category count.

3. **Diverse large-scale benchmark for 9D pose foundation models.** We establish standardized symmetry-aware evaluation protocols and provide baseline models for Every9D-21M. Training on Every9D-21M improves performance on PASCAL3D+ and ImageNet3D, while yielding substantially stronger generalization to HANDAL than training on ImageNet3D.

2 Related Work

In this section, we review prior work on 9D object pose annotation from real-world imagery, organizing the literature according to the level of annotation effort involved. We identify four principal paradigms: (a) methods based on manual image-level pose annotations; (b) techniques leveraging video-level annotations to exploit multi-view consistency across frames; (c) video-reference-level annotation schemes, where pose information is defined with respect to a shared reference video and propagated across others; (d) self-supervised approaches that avoid explicit human pose annotations. In Table 1, we compare quantitatively real-world datasets with 9D pose annotations.

2.1 Image-Level Pose Annotations

Obtaining pose annotations at the image level is arguably the most labor-intensive and technically challenging paradigm. Prior works [56, 55, 33] typically follow a similar protocol: an exemplary CAD mesh is selected for a given category and manually aligned to each image by adjusting its pose parameters. While this strategy facilitates annotations, it is inherently sensitive to discrepancies between the chosen template mesh and the true object. In particular, if the mesh proportions deviate from the real object, the projected alignment can appear accurate in the 2D image plane while remaining geometrically inconsistent in 3D, leading to systematic pose errors. Given scale ambiguity and the absence of real-world camera intrinsics, these approaches evaluate only 3D object orientations.

Among these efforts, ImageNet3D [33] represents the largest image-level annotated benchmark, comprising approximately 86K images. In contrast, our approach scales to 21.8M annotated images while requiring only around 1K manual pose annotations, substantially reducing human effort while increasing dataset scale by nearly two orders of magnitude.

Beyond the pose annotation paradigms discussed above, WildDet3D [18] annotates 3D bounding boxes at the image level, where object orientation is defined primarily by the gravity direction. In contrast, our approach leverages semantically grounded cross-category intrinsic and interactive orientation rules, detailed in the supplementary material.

2.2 Video-Level Pose Annotations

Video-level annotation strategies reduce ambiguity by exploiting multi-view consistency across frames. In the simplest setting, where each video contains a single object instance, the required human effort scales approximately with the number of videos. Prominent examples include Objectron [1], Wild6D [13], and HANDAL [17]. Objectron relies on manual pose annotation at the video level, while Wild6D and HANDAL adopt semi-automatic pipelines: Wild6D annotates keyframes and propagates poses to the remaining frames using ICP-based alignment, whereas HANDAL initializes poses with a tracker and subsequently applies manual refinement at the frame level.

More complex settings involve scenes with multiple objects and object instances reappearing across different videos. In such cases, the annotation effort scales with both the number of videos and the number of objects per scene. NOCS-REAL275 [48] relies entirely on manual labeling. PhoCal [50] and HouseCat6D [21] follow semi-automatic procedures in which previously scanned objects, acquired via structured-light scanning, are matched to scene observations using correspondences obtained with a robot arm equipped with a measurement probe to determine keypoint locations.

Despite leveraging videos to propagate annotations across frames, labeling each object instance within a sequence remains labor-intensive. In terms of scale, Objectron [1] is the largest dataset by number of annotated objects, comprising approximately 17K instances, but it covers only 9 categories. This category diversity is nearly two orders of magnitude smaller than ours, which spans 700 categories. The second-largest dataset in terms of object instances, Omni6DPose-ROPE [62], contains only 581 objects, which is nearly two orders of magnitude smaller than our 109K annotated objects.

Table 1: Comparison of real-world model-free pose datasets. *Note that depth estimates in our dataset are obtained using a monocular depth prediction method [58] and are subsequently aligned with SfM.

| Dataset | In-/Outdoor | Modality | Eval. | #Categories | #Objects | #Videos | #Images | #Manual |
|----------------------|-------------|----------|-------|-------------|-------------|-------------|--------------|---------|
| PASCAL3D+ [56] | ✓ | RGB | 3D | 12 | 12K | / | 12K | 12K |
| ObjectNet3D [55] | ✓ | RGB | 3D | 100 | 57K | / | 57K | 57K |
| ImageNet3D [33] | ✓ | RGB | 3D | 200 | 86K | / | 86K | 86K |
| Objectron [1] | ✓ | RGB | 9D | 9 | 17K | 15K | 4M | 17K |
| Wild6D [13] | ✓ | RGBD | 9D | 5 | 162 | 486 | 10K | 162 |
| HANDAL [17] | ✓ | RGBD | 9D | 17 | 212 | 2K | 308K | 2K |
| NOCS-REAL275 [48] | × | RGBD | 9D | 6 | 42 | 18 | 8K | 90 |
| PhoCaL [50] | × | RGBD | 9D | 8 | 60 | 24 | 3.9K | 60 |
| HouseCat6D [21] | × | RGBD | 9D | 10 | 194 | 41 | 23.5K | 4.8K |
| Omni6DPose-ROPE [62] | × | RGBD | 9D | 149 | 581 | 363 | 332K | 1.8K |
| Every9D-21M (Ours) | ✓ | RGBD* | 9D | 700 | 109K | 109K | 21.8M | 1K |

uCO3D [30] performs scene-level normalization of object-centric reconstructions by enforcing a gravity-aligned vertical axis, normalizing scale and translation, and resolving horizontal orientation using PCA. While this removes the arbitrary coordinate frames commonly produced by structure-from-motion pipelines, it does not guarantee semantic object orientation. In particular, the vertical scene axis does not necessarily correspond to the semantic top–bottom direction of the object, and PCA-based yaw alignment is not semantic either. In contrast, our work focuses on semantic canonicalization, aligning objects according to meaningful orientation rules across instances.

2.3 Reference-Level Pose Annotations

To the best of our knowledge, methods exploiting automatic cross-instance alignment remain limited [44, 4, 20]. The first method aligning instances to a single reference [44] is limited to 1K videos across 23 categories, applies no filtering to remove incorrect poses after alignment, and requires category-level information to select a reference. C3PO [4] canonicalizes 200 videos across 20 categories using category supervision. It extends single-reference canonicalization to partially observed objects through pairwise all-to-all instance alignment, whose quadratic complexity limits scalability.

More recently, Jin et al. [20] canonicalize a filtered subset of 32K clean 3D assets from Objaverse using one annotated reference per category. This again assumes access to category information, and the alignment method has not been shown to generalize to real-world videos. In particular, the support-plane strategy is questionable for videos with noisy, partial point clouds reconstructed via structure-from-motion and imperfect masks.

In contrast, our method does not rely on category information, allowing cross-instance alignment even across categories and thereby reducing human effort.

2.4 Self-Supervised Pose Annotations

MagicPony [53] advances self-supervised 6D pose and shape recovery from real-world data, focusing on articulated animal categories. However, it does not provide a quantitative evaluation of 6D pose accuracy, and its generalization to rigid everyday objects remains unexplored.

Purely geometric self-supervised approaches [24, 41] have so far demonstrated strong performance primarily on a limited set of object categories, such as airplanes, cars, and bottles, and typically under the assumption of complete point cloud observations. In scenarios involving partial point clouds, their pose estimation accuracy degrades substantially. Furthermore, [20] shows that Condor [41] exhibits particularly poor performance in low-instance regimes. Given the long-tailed distribution of object instances in real-world data, as well as the inherent noise introduced by structure-from-motion reconstruction and imperfect object masks, these limitations become critical in our setting.

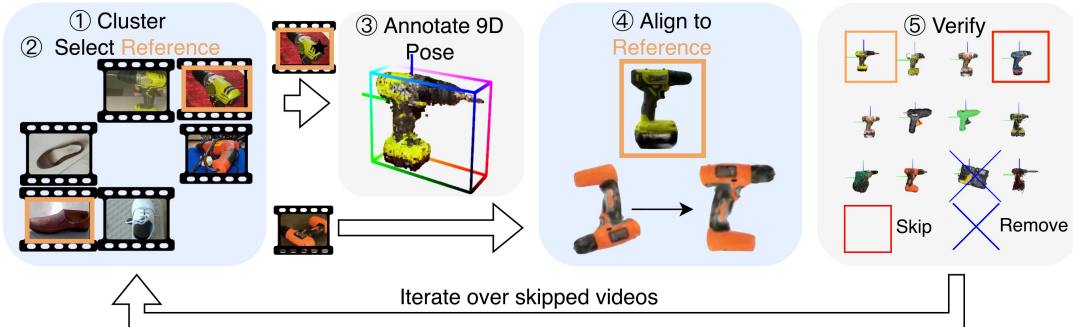


Figure 2: **Canonicalization Framework.** Our framework to canonicalize object-centric videos consists of 5 steps. 1) We cluster all object-centric videos. 2) We select a reference per cluster. 3) We annotate a 9D pose for the reference. 4) We align each object to its reference based upon geometry and appearance. 5) We verify all objects, removing objects with bad reconstruction and skipping objects with wrong pose annotation. Next, we repeat all steps over all skipped videos. Also note that manual labour is only required for step 3) 9D Pose annotation of the reference and 5) verification.

3 Method

Our objective is to obtain large-scale, high-quality 9D pose annotations for real-world object-centric videos. To scale annotation while maintaining consistent object orientation across instances, we adopt a reference-based canonicalization strategy: a small set of manually annotated reference objects defines canonical coordinate frames that are automatically propagated to many object instances and corresponding video frames through cross-instance and multi-view alignment.

Our complete framework comprises five stages. First, we cluster object-centric videos (Section 3.1). Second, we select a representative reference instance per cluster (Section 3.2). Third, we manually annotate the 9D pose of the selected reference (Section 3.3). Fourth, we align all remaining videos within the cluster to the corresponding reference (Section 3.4). Finally, we verify the propagated pose annotations (Section 3.5). After processing one cluster, we proceed iteratively with the remaining videos. An overview of the full pipeline is provided in Figure 2. Beyond generating high-quality 9D pose annotations, we additionally train a 9D pose estimation network as a baseline model. The architecture and training procedure are described in Section 3.7.

3.1 Clustering Videos

The inputs to this stage are object-centric videos recorded by non-experts, typically capturing the object from diverse viewpoints, often close to a full 360° around it. These videos exhibit substantial variation in distance, elevation, illumination, background clutter, and motion blur.

To assign videos to clusters sharing a common reference instance, we compute a single embedding per video. Specifically, we extract DINOv3 [42] features from a small set of uniformly sampled frames and average them after normalization. Empirically, averaging only a few frames performs comparably to using many more on the CO3D benchmark while being substantially more efficient. We then cluster the normalized video embeddings using k-means with cosine distance, where k determines the number of clusters.

To validate our clustering strategy, we evaluate it on a small subset of the CO3D benchmark [40] with annotated 3D poses [17], see Table 2. Category-agnostic clustering achieves downstream alignment accuracy close to grouping videos by ground-truth category labels, indicating near category-level cluster quality. Unlike category-based grouping, clustering offers additional flexibility: the number of clusters can be adjusted to control the number of reference objects requiring manual annotation, which is especially

Table 2: **Canonicalization design validation** on annotated CO3D.

| # | Method | Cat.-agn. | Ref. | Iter. | GT / iter. | Acc@30° ↑ |
|---|-----------|-----------|--------|-------|------------|--------------|
| 1 | UOP3D[44] | × | Random | — | 10% | 82.2% |
| 2 | Ours | ✓ | Random | — | 10% | 76.1% |
| 3 | Ours | ✓ | Medoid | — | 10% | 83.0% |
| 4 | Ours | ✓ | Medoid | 2 | 5% | 86.5% |

relevant given the dataset size. Moreover, clustering mitigates the impact of incorrect category labels. Finally, it enables leveraging cross-category visual similarities across objects, rather than relying solely on verbal categories. As reported in Table 2, performing two alignment iterations on only half of the ground-truth pose annotations improves performance through cross-category alignment. Notably, these gains are observed even though the subset exhibits low category overlap and limited sample diversity.

3.2 Reference Selection

In contrast to prior work [44], we do not select a random reference. Instead, we choose the cluster medoid, i.e., the video whose image-feature embedding has the smallest average distance to all other videos in the cluster. This yields a more representative reference object and has shown to significantly improve accuracy on the CO3D benchmark, see Table 2.

3.3 9D Pose Annotation

To annotate an object-centric video we first obtain camera poses and a sparse 3D point cloud using VGGSFm [49]. To extract the object of interest, we apply multi-view masking as in [44]. Therefore, we use masks from text-conditioned LangSAM [23, 35], with temporal stabilization using XMem [3].

By fitting a centered oriented 3D bounding box to the masked point cloud, we obtain a 9D pose annotation for each 3D orientation annotation, thereby reducing the effort. To achieve high-precision, we developed an interactive tool that operates directly on the masked point clouds. Annotators first place axes coarsely, then refine them with precise incremental controls (1°). Finally, all labels were cross-verified by another annotator in a separate review pass to ensure quality and consistency.

Since object orientation must be defined consistently across instances, we establish a set of cross-category orientation rules (detailed in the supplementary material). Concretely, we define oriented object axes according to three guiding principles: (a) *intrinsic orientation*, such as a natural mounting direction (e.g., wall-mounted objects) or the primary direction of motion; (b) *human-object interaction*, capturing whether an object is typically facing toward or away from the user, as well as how it is naturally grasped or held during use; and (c) *object-object interaction*, reflecting functional usage patterns, such as painting direction or squeezing direction. For example, the canonical front of a chair is defined as the direction opposite to the backrest, while for tools such as scissors the canonical forward axis aligns with the cutting direction. These simple yet systematic rules allow us to define consistent canonical orientations across diverse object categories.

3.4 Alignment to Reference

Our goal is to estimate the rigid transformation that aligns the reconstructed object instance with the canonical reference instance of the cluster. To align an object-centric video to a reference instance, we jointly leverage geometric structure and visual appearance. Each video is represented as a 3D surface endowed with DINO features [42] projected onto a reconstructed mesh, following [44].

From the masked sparse reconstruction Section 3.3, we estimate a coarse object surface via alpha shapes [11]. Multi-view DINO features are then projected onto the resulting mesh. This results in a surface feature representation $\mathcal{S} = \{\mathcal{V}, \mathcal{F}\}$, with the vertices $\mathcal{V} = \{\mathbf{v}_i \in \mathbb{R}^3\}_{i=1}^{|\mathcal{V}|}$, and the multi-view features $\mathcal{F} = \left\{ \left\{ \mathbf{f}_i^k \in \mathbb{R}^D \right\}_{k=1}^{|\mathcal{F}_i|} \right\}_{i=1}^{|\mathcal{V}|}$. Here, \mathbf{f}_i^k denotes the k -th feature observation of vertex i .

Given two surface representations \mathcal{S}_i and \mathcal{S}_j , we estimate their relative alignment T , which is composed of rotation, translation and scale, using RANSAC initialization followed by gradient-based refinement, as in [44]. The alignment minimizes a weighted combination of geometric and appearance distances: $\text{dist}(\mathcal{S}_i, \mathcal{S}_j) = (1 - \alpha) \text{dist}_{\text{geo}}(\mathcal{S}_i, \mathcal{S}_j) + \alpha \text{dist}_{\text{app}}(\mathcal{S}_i, \mathcal{S}_j)$, where $\alpha \in [0, 1]$ controls the trade-off between geometry and appearance. In practice, we set $\alpha = 0.2$.

The geometric term dist_{geo} is defined as a weighted Chamfer distance between vertices. Similarly, the appearance term dist_{app} is evaluated in 3D space, however, nearest neighbors are determined in feature space rather than spatial proximity.

Specifically, for each vertex i , we identify the target vertex whose associated feature set yields the smallest aggregated nearest-neighbor feature distance: $\mathbf{v}_{\text{nn}}^{\text{feat}}(i) =$

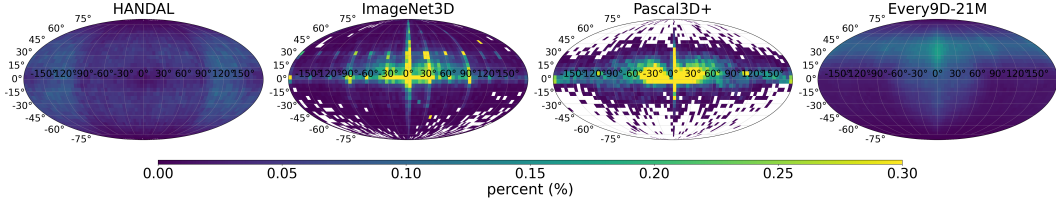


Figure 3: **Mollweide projection of camera-direction histograms in the canonical object frame** Every9D-21M is the only dataset providing broad, near-uniform coverage of the viewing sphere; ImageNet3D and Pascal3D+ concentrate sharply along the equator (canonical photograph angles), while HANDAL covers the hemisphere uniformly but contains very few categories.

$\arg \min_{j \in \{1, \dots, |\mathcal{V}_j|\}} \sum_l \min_k \|\mathbf{f}_j^k - \mathbf{f}_i^l\|_2$, for $i \in \{1, \dots, |\mathcal{V}_i|\}$. The bi-directional appearance distance is then computed between the corresponding 3D vertex locations. Each vertex-level correspondence is weighted according to its feature-space correspondence cycle consistency as defined [44]. The resulting transformation aligns the instance to the reference coordinate frame. Further, we fit an oriented 3D bounding box to the instance’s masked point cloud and retrieve the 9D pose, which is propagated to all frames of the video.

3.5 9D Pose Verification

For each sequence, we visualize the canonicalized 3D reconstruction from three canonical views (front/top/right) and inspect whether the predicted pose is accurate and consistent with the object’s semantic axes. Additionally, we visually examine reconstruction quality.

We categorize failures into two groups. **Filtered** sequences are permanently removed from the dataset because the underlying geometry is unreliable, e.g., due to poor reconstruction quality (moving objects, strong noise, missing parts) or because the masked reconstruction contains multiple object instances (object leakage or multiple identical objects within the mask). **Skipped** sequences are kept for later processing because the failure is caused by the chosen reference or pose rather than the raw geometry. Common reasons include overly diverse clusters where the medoid reference remains too far from many members, and geometric mismatches from fine-grained state changes (e.g., open vs. closed scissors) where alignment becomes ambiguous. We also observe occasional reference failures where semantically different objects are clustered together (e.g., a spoon aligned to a pan), leading to systematic misalignment and requiring skipping and re-clustering.

3.6 Iterative Process

We apply the pipeline iteratively. After the first pass, we remove filtered sequences and re-process the skipped subset by re-clustering, selecting new references, annotating poses, and repeating alignment and verification. Overall, we annotate 1000 reference objects (across all iterations), and leverage clustering to control this annotation budget: by choosing the number of clusters, we can trade off cluster granularity against the number of references that require 3D pose annotation.

3.7 Monocular 9D Pose Estimation

To demonstrate the usefulness of Every9D-21M for training monocular pose estimators, we train a simple baseline model for 9D pose prediction. Following prior work [47, 62, 61], we fuse geometric and appearance information by re-projecting each pixel into 3D using its depth and attaching its patch feature. Instead of adopting PointNet++ [39] or DGCNN [38, 59, 61] as the point cloud backbone, we employ LitePT [60], a lightweight architecture that combines sparse 3D convolutions [15] with point transformer layers [54] to achieve efficient feature aggregation. For image encoding, we use a pretrained DINO backbone [36]. The encoded image and geometric features are concatenated and passed through a two-layer MLP, which projects the representation into a 12D pose embedding space, consisting of 3D object translation, 3D object size, and 6D rotation [68]. For the rotation we employ a geodesic loss, while for the 3D translation and the 3D object extent we apply an ℓ_1 loss.

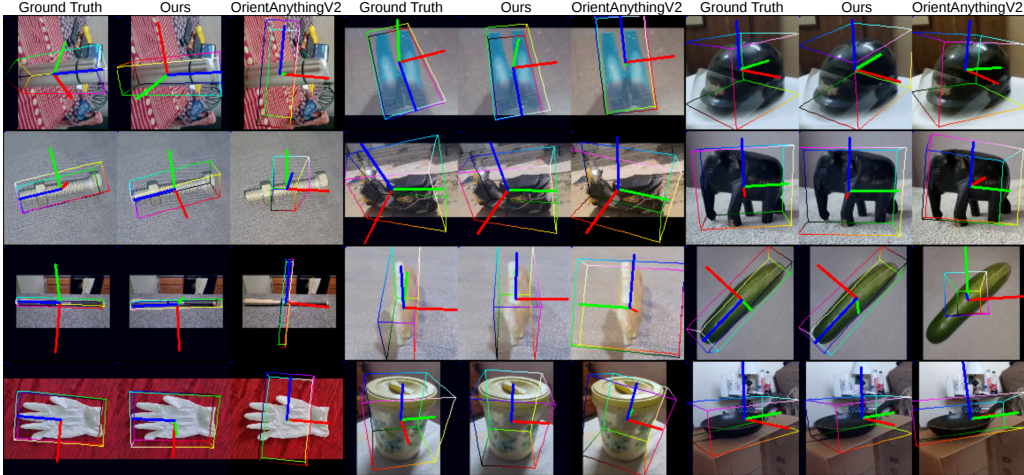


Figure 4: **Qualitative Results on Every9D-21M (test split)**. Since OrientAnythingV2 does not predict 3D bounding boxes, we visualize its rotation estimates using ground-truth 3D boxes. Predicted axes are color-coded as red (left), green (back), and blue (top).

4 Dataset

We present a comprehensive overview of our dataset, which comprises 21.8M images, 109K annotated objects, and 700 categories across many super-categories. Its distribution is visualized in Figure S6. As shown, the dataset exhibits broad semantic coverage, spanning diverse domains from indoor to outdoor object categories, thereby capturing substantial real-world diversity. Importantly, the category distribution remains largely unchanged, with only minor deviations from the original dataset. These changes primarily affect categories such as animals, where dynamic videos break the assumption of a single consistent coordinate frame, and meals, which often contain multiple small objects.

Figure 3 illustrates the viewpoint distribution of the canonicalized objects. The dataset provides coverage from all viewing directions, indicating that objects are well represented across the full pose sphere. A slight bias toward frontal views and viewpoints mildly elevated above the horizontal plane is observable. This tendency can be attributed to common recording conditions in real-world videos: many objects naturally rest or are positioned upright (e.g., bicycles), or are placed such that their frontal surface faces upward (e.g., books). Consequently, front-facing and slightly top-down perspectives occur more frequently, while overall maintaining broad viewpoint diversity.

5 Experiments

We validate the key design choices underlying our canonicalization framework for constructing Every9D-21M in Table 2. Furthermore, we partition Every9D-21M into disjoint training and test splits. As shown in Table 3, Every9D-21M: (a) introduces a novel large-scale and challenging benchmark on which models trained with our dataset substantially outperform prior foundation models, including OrientAnythingV1, OrientAnythingV2, and WildDet3D; (b) complements ImageNet3D within the ImageNet3D domain; and (c) demonstrates stronger generalization to HANDAL, despite the considerable domain gap, compared to models trained solely on ImageNet3D.

5.1 Experimental Details

Train–Test Split. Every9D-21M contains 905 categories in total. For evaluation, we retain only categories with at least 10 object-centric videos, resulting in a test set of 700 categories.

Symmetry-Aware Evaluation. The cross-category orientation rules (Section S10) enable the identification of category-level symmetries through unconstrained orientations. For example, a bottle is defined only by its containment direction, inducing continuous rotational symmetry, while a spatula specifies a front-to-back axis instead of direction, resulting in discrete rotational symmetry.

| Dataset | PASCAL3D | | ImageNet3D | | HANDAL | | | Every9D-test | | |
|---------------------------|-------------|-------------|-------------|-------------|-------------|-------------|-------------|--------------|-------------|-------------|
| | Acc@30° | | Acc@30° | | Acc@30° | 3D IoU | | Acc@30° | | 3D IoU |
| Symmetry-Aware | × | ✓ | × | ✓ | × | ✓ | | × | ✓ | |
| OrientAnythingV1 [51] | 67.9 | 72.4 | 41.6 | 48.4 | 2.9 | 7.4 | – | 18.6 | 37.5 | – |
| OrientAnythingV2 [52] | 88.2 | 92.2 | 55.7 | 62.7 | 2.1 | 3.8 | – | 23.8 | 46.1 | – |
| WildDet3D [18] | – | – | – | – | 0.2 | 0.4 | 6.6 | 1.5 | 6.5 | 23.7 |
| Ours (Every9D) | 50.6 | 60.0 | 27.4 | 34.9 | 12.3 | 23.6 | 25.0 | 40.4 | 63.8 | 50.5 |
| Ours (ImageNet3D) | 83.8 | 86.7 | <u>58.0</u> | <u>62.8</u> | 2.8 | 2.9 | – | 10.2 | 10.2 | – |
| Ours (Every9D+ImageNet3D) | <u>87.7</u> | <u>90.3</u> | 59.0 | 64.2 | <u>8.5</u> | <u>16.4</u> | <u>23.2</u> | <u>33.7</u> | <u>56.7</u> | <u>47.2</u> |

Table 3: **Quantitative Results Across Datasets.** We evaluate rotational accuracy at both coarse (30°) thresholds, in addition to the average 3D IoU. We compare our approach against OrientAnythingV1, OrientAnythingV2, and WildDet3D. Note that OrientAnythingV1 and OrientAnythingV2 predict object rotation only and do not estimate 3D bounding boxes.

5.2 Comparison with Prior Work

Every9D-21M is a novel large-scale benchmark. As shown in Table 3, Every9D-21M poses a substantial challenge even for the state-of-the-art foundation models. Our model trained on Every9D-21M-train outperforms OrientAnythingV2 in coarse rotation (30°) accuracy by **16.6** points in the symmetry-unaware setting and **17.7** points in the symmetry-aware setting. Since the training code of OrientAnythingV2 is unavailable, we compare against the released model trained on 600K reconstructed 3D assets and ImageNet3D. The qualitative comparisons in Figure 4 highlight three key advantages of our approach over OrientAnythingV2: improved robustness to unusual object orientations, more accurate estimation of subtle angular differences, and stronger resilience under challenging lighting conditions. Furthermore, WildDet3D orientations appear strongly biased by gravity, resulting in poor rotation accuracy. Our model additionally outperforms WildDet3D by **26.8** points in 3D IoU.

Every9D-21M complements ImageNet3D in the ImageNet3D domain. We observe that jointly training our model with mixed batches, where half of each batch is sampled from Every9D-21M-train, consistently improves performance on both ImageNet3D and PASCAL3D+. For this setting, we obtain segmentation masks using SAM [23], prompted with the 2D bounding boxes, and estimate depth with DepthAnythingV3 [25]. Since the scene scale is not aligned with the predicted depth, we only calculate the orientation loss for the subset of the batch containing ImageNet3D samples.

Every9D-21M generalizes better to HANDAL than ImageNet3D. Despite the significant domain gap between Every9D-21M and HANDAL, including predicted versus sensor depth and stronger occlusions, training on Every9D-21M yields substantially better generalization than ImageNet3D. In particular, Every9D-21M-train improves coarse (30°) accuracy by **20.7** percentage points.

6 Limitations

While Every9D-21M substantially scales real-world 9D pose supervision, several limitations remain.

Symmetry handling at training time. Our evaluation accounts for category-level symmetries, but the baseline model itself predicts a single deterministic pose per image. Modeling symmetry-induced ambiguity through multi-hypothesis or distributional predictions is a promising direction for improving performance on rotationally symmetric categories.

Depth and dynamics. Depth annotations are inherited from monocular DepthAnythingV2 [58] estimates rather than ground-truth sensor depth, with scale aligned to the structure-from-motion reconstruction. The dataset also does not cover dynamic object interactions: each video is assumed to capture a static instance from multiple viewpoints. A promising direction for future work is to decouple dynamic videos into 3D reconstruction and 9D pose estimation with respect to an arbitrary world frame, enabling our category-level alignment framework to operate on object-level 3D reconstructions extracted from non-static scenes.

7 Conclusion

We introduced **Every9D-21M**, a dataset of 9D pose annotations for 21.8M real-world images across 700 everyday object categories, derived from 109K object-centric videos via a reference-based canonicalization framework with full human verification of every propagated pose. Beyond establishing symmetry-aware evaluation protocols and baselines, we show that training on Every9D-21M improves performance on PASCAL3D+ and ImageNet3D, while achieving substantially stronger transfer to HANDAL than training on ImageNet3D alone.

Acknowledgments

AK acknowledges support via his Emmy Noether Research Group funded by the German Research Foundation (DFG) under grant number 468670075. This research was funded by the Deutsche Forschungsgemeinschaft (DFG, German Research Foundation) under grant number 539134284, through EFRE (FEIH_2698644) and the state of Baden-Württemberg.



Baden-Württemberg



Co-funded by
the European Union

References

- [1] Ahmadyan, A., Zhang, L., Ablavatski, A., Wei, J., Grundmann, M.: Objectron: A large scale dataset of object-centric videos in the wild with pose annotations. In: Proceedings of the IEEE/CVF conference on computer vision and pattern recognition. pp. 7822–7831 (2021)
- [2] Chen, K., Dou, Q.: Sgpa: Structure-guided prior adaptation for category-level 6d object pose estimation. In: Proceedings of the IEEE/CVF international conference on computer vision. pp. 2773–2782 (2021)
- [3] Cheng, H.K., Schwing, A.G.: Xmem: Long-term video object segmentation with an atkinson-shiffrin memory model. In: European conference on computer vision. pp. 640–658. Springer (2022)
- [4] Chi, Y., Sommer, L., Dünkel, O., Muhle, D., Cremers, D., Theobalt, C., Kortylewski, A.: C3PO: Canonicalization of 3d pose from partial views with generalizable correspondence features. In: Thirteenth International Conference on 3D Vision (2026)
- [5] Choy, C.B., Xu, D., Gwak, J., Chen, K., Savarese, S.: 3d-r2n2: A unified approach for single and multi-view 3d object reconstruction. In: European conference on computer vision. pp. 628–644. Springer (2016)
- [6] Collins, J., Goel, S., Deng, K., Luthra, A., Xu, L., Gundogdu, E., Zhang, X., Vicente, T.F.Y., Dideriksen, T., Arora, H., et al.: Abo: Dataset and benchmarks for real-world 3d object understanding. In: Proceedings of the IEEE/CVF conference on computer vision and pattern recognition. pp. 21126–21136 (2022)
- [7] Deitke, M., Liu, R., Wallingford, M., Ngo, H., Michel, O., Kusupati, A., Fan, A., Laforte, C., Voleti, V., Gadre, S.Y., et al.: Objaverse-xl: A universe of 10m+ 3d objects. Advances in Neural Information Processing Systems **36**, 35799–35813 (2023)
- [8] Deitke, M., Schwenk, D., Salvador, J., Weihs, L., Michel, O., VanderBilt, E., Schmidt, L., Ehsani, K., Kembhavi, A., Farhadi, A.: Objaverse: A universe of annotated 3d objects. In: Proceedings of the IEEE/CVF conference on computer vision and pattern recognition. pp. 13142–13153 (2023)
- [9] Deng, Y., Yang, J., Tong, X.: Deformed implicit field: Modeling 3d shapes with learned dense correspondence. In: Proceedings of the IEEE/CVF Conference on Computer Vision and Pattern Recognition. pp. 10286–10296 (2021)

- [10] Dünkel, O., Wimmer, T., Theobalt, C., Rupperecht, C., Kortylewski, A.: Do it yourself: Learning semantic correspondence from pseudo-labels. In: Proceedings of the IEEE/CVF International Conference on Computer Vision. pp. 5834–5844 (2025)
- [11] Edelsbrunner, H., Mücke, E.P.: Three-dimensional alpha shapes. *ACM Transactions On Graphics (TOG)* **13**(1), 43–72 (1994)
- [12] Fu, H., Jia, R., Gao, L., Gong, M., Zhao, B., Maybank, S., Tao, D.: 3d-future: 3d furniture shape with texture. *International Journal of Computer Vision* **129**(12), 3313–3337 (2021)
- [13] Fu, Y., Wang, X.: Category-level 6d object pose estimation in the wild: A semi-supervised learning approach and a new dataset. *Advances in Neural Information Processing Systems* **35**, 27469–27483 (2022)
- [14] Goodwin, W., Vaze, S., Havoutis, I., Posner, I.: Zero-shot category-level object pose estimation. In: *European Conference on Computer Vision*. pp. 516–532. Springer (2022)
- [15] Graham, B., Engelcke, M., Van Der Maaten, L.: 3d semantic segmentation with submanifold sparse convolutional networks. In: *Proceedings of the IEEE conference on computer vision and pattern recognition*. pp. 9224–9232 (2018)
- [16] Groueix, T., Fisher, M., Kim, V.G., Russell, B.C., Aubry, M.: A papier-mâché approach to learning 3d surface generation. In: *Proceedings of the IEEE conference on computer vision and pattern recognition*. pp. 216–224 (2018)
- [17] Guo, A., Wen, B., Yuan, J., Tremblay, J., Tyree, S., Smith, J., Birchfield, S.: Handal: A dataset of real-world manipulable object categories with pose annotations, affordances, and reconstructions. In: *2023 IEEE/RSJ International Conference on Intelligent Robots and Systems (IROS)*. pp. 11428–11435. IEEE (2023)
- [18] Huang, W., Zhang, J., Li, S., Jia, T., Duan, J., Cheng, Y., Cho, J., Wallingford, M., Soraki, R., Kim, C.D., et al.: Wilddet3d: Scaling promptable 3d detection in the wild. *arXiv preprint arXiv:2604.08626* (2026)
- [19] Jesslen, A., Zhang, G., Wang, A., Ma, W., Yuille, A., Kortylewski, A.: Novum: Neural object volumes for robust object classification. In: *European Conference on Computer Vision*. pp. 264–281. Springer (2024)
- [20] Jin, L., Wang, Y., Chen, W., Dai, Q., Gao, Q., Qin, X., Chen, B.: One-shot 3d object canonicalization based on geometric and semantic consistency. In: *Proceedings of the Computer Vision and Pattern Recognition Conference*. pp. 16850–16859 (2025)
- [21] Jung, H., Wu, S.C., Ruhkamp, P., Zhai, G., Schieber, H., Rizzoli, G., Wang, P., Zhao, H., Garattoni, L., Meier, S., et al.: Housecat6d-a large-scale multi-modal category level 6d object perception dataset with household objects in realistic scenarios. In: *Proceedings of the IEEE/CVF Conference on Computer Vision and Pattern Recognition*. pp. 22498–22508 (2024)
- [22] Khanna, M., Mao, Y., Jiang, H., Haresh, S., Shacklett, B., Batra, D., Clegg, A., Undersander, E., Chang, A.X., Savva, M.: Habitat synthetic scenes dataset (hssd-200): An analysis of 3d scene scale and realism tradeoffs for objectgoal navigation. In: *Proceedings of the IEEE/CVF Conference on Computer Vision and Pattern Recognition*. pp. 16384–16393 (2024)
- [23] Kirillov, A., Mintun, E., Ravi, N., Mao, H., Rolland, C., Gustafson, L., Xiao, T., Whitehead, S., Berg, A.C., Lo, W.Y., et al.: Segment anything. In: *Proceedings of the IEEE/CVF international conference on computer vision*. pp. 4015–4026 (2023)
- [24] Li, X., Weng, Y., Yi, L., Guibas, L.J., Abbott, A., Song, S., Wang, H.: Leveraging se(3) equivariance for self-supervised category-level object pose estimation from point clouds. *Advances in neural information processing systems* **34**, 15370–15381 (2021)
- [25] Lin, H., Chen, S., Liew, J., Chen, D.Y., Li, Z., Shi, G., Feng, J., Kang, B.: Depth anything 3: Recovering the visual space from any views. *arXiv preprint arXiv:2511.10647* (2025)

- [26] Lin, Y., Tremblay, J., Tyree, S., Vela, P.A., Birchfield, S.: Single-stage keypoint-based category-level object pose estimation from an rgb image. In: 2022 International Conference on Robotics and Automation (ICRA). pp. 1547–1553. IEEE (2022)
- [27] Liu, J., Chen, Y., Ye, X., Qi, X.: Ist-net: Prior-free category-level pose estimation with implicit space transformation. In: Proceedings of the IEEE/CVF International Conference on Computer Vision. pp. 13978–13988 (2023)
- [28] Liu, M., Shi, R., Kuang, K., Zhu, Y., Li, X., Han, S., Cai, H., Porikli, F., Su, H.: Openshape: Scaling up 3d shape representation towards open-world understanding. *Advances in neural information processing systems* **36**, 44860–44879 (2023)
- [29] Liu, Q., Zhang, Y., Bai, S., Kortylewski, A., Yuille, A.: Direct-3d: Learning direct text-to-3d generation on massive noisy 3d data. In: Proceedings of the IEEE/CVF Conference on Computer Vision and Pattern Recognition. pp. 6881–6891 (2024)
- [30] Liu, X., Tayal, P., Wang, J., Zarzar, J., Monnier, T., Tertikas, K., Duan, J., Toisoul, A., Zhang, J.Y., Neverova, N., et al.: Uncommon objects in 3d. In: Proceedings of the IEEE/CVF Conference on Computer Vision and Pattern Recognition. pp. 14102–14113 (2025)
- [31] Loshchilov, I., Hutter, F.: Decoupled weight decay regularization. arXiv preprint arXiv:1711.05101 (2017)
- [32] Lu, Y., Tian, Y., Jiang, Z., Zhao, Y., Yang, Y., Ouyang, H., Hu, H., Yu, H., Shen, Y., Liao, Y.: Orientation matters: Making 3d generative models orientation-aligned. arXiv preprint arXiv:2506.08640 (2025)
- [33] Ma, W., Zhang, G., Liu, Q., Zeng, G., Kortylewski, A., Liu, Y., Yuille, A.: Imagenet3d: Towards general-purpose object-level 3d understanding. *Advances in Neural Information Processing Systems* **37**, 96127–96149 (2024)
- [34] Mariotti, O., Mac Aodha, O., Bilen, H.: Improving semantic correspondence with viewpoint-guided spherical maps. In: Proceedings of the IEEE/CVF Conference on Computer Vision and Pattern Recognition. pp. 19521–19530 (2024)
- [35] Medeiros, L.: lang-segment-anything. <https://github.com/luca-medeiros/lang-segment-anything> (2023), gitHub repository
- [36] Oquab, M., Darcet, T., Moutakanni, T., Vo, H., Szafraniec, M., Khalidov, V., Fernandez, P., Haziza, D., Massa, F., El-Nouby, A., et al.: Dinov2: Learning robust visual features without supervision. arXiv preprint arXiv:2304.07193 (2023)
- [37] Park, J.J., Florence, P., Straub, J., Newcombe, R., Lovegrove, S.: Deepsdf: Learning continuous signed distance functions for shape representation. In: Proceedings of the IEEE/CVF conference on computer vision and pattern recognition. pp. 165–174 (2019)
- [38] Phan, A.V., Le Nguyen, M., Nguyen, Y.L.H., Bui, L.T.: Dgcnn: A convolutional neural network over large-scale labeled graphs. *Neural Networks* **108**, 533–543 (2018)
- [39] Qi, C.R., Yi, L., Su, H., Guibas, L.J.: Pointnet++: Deep hierarchical feature learning on point sets in a metric space. *Advances in neural information processing systems* **30** (2017)
- [40] Reizenstein, J., Shapovalov, R., Henzler, P., Sbordone, L., Labatut, P., Novotny, D.: Common objects in 3d: Large-scale learning and evaluation of real-life 3d category reconstruction. In: Proceedings of the IEEE/CVF international conference on computer vision. pp. 10901–10911 (2021)
- [41] Sajnani, R., Poulénard, A., Jain, J., Dua, R., Guibas, L.J., Sridhar, S.: Condor: Self-supervised canonicalization of 3d pose for partial shapes. In: Proceedings of the IEEE/CVF Conference on Computer Vision and Pattern Recognition. pp. 16969–16979 (2022)
- [42] Siméoni, O., Vo, H.V., Seitzer, M., Baldassarre, F., Oquab, M., Jose, C., Khalidov, V., Szafraniec, M., Yi, S., Ramamonjisoa, M., et al.: Dinov3. arXiv preprint arXiv:2508.10104 (2025)

- [43] Sommer, L., Dünkel, O., Theobalt, C., Kortylewski, A.: Common3d: Self-supervised learning of 3d morphable models for common objects in neural feature space. In: Proceedings of the Computer Vision and Pattern Recognition Conference. pp. 6468–6479 (2025)
- [44] Sommer, L., Jesslen, A., Ilg, E., Kortylewski, A.: Unsupervised learning of category-level 3d pose from object-centric videos. In: Proceedings of the IEEE/CVF Conference on Computer Vision and Pattern Recognition. pp. 22787–22796 (2024)
- [45] Stark, M., Goesele, M., Schiele, B.: Back to the future: Learning shape models from 3d cad data. In: Bmvc. vol. 2, p. 5 (2010)
- [46] Sun, S., Han, K., Kong, D., Tang, H., Yan, X., Xie, X.: Topology-preserving shape reconstruction and registration via neural diffeomorphic flow. In: Proceedings of the IEEE/CVF Conference on Computer Vision and Pattern Recognition. pp. 20845–20855 (2022)
- [47] Wang, C., Xu, D., Zhu, Y., Martín-Martín, R., Lu, C., Fei-Fei, L., Savarese, S.: Densefusion: 6d object pose estimation by iterative dense fusion. In: Proceedings of the IEEE/CVF conference on computer vision and pattern recognition. pp. 3343–3352 (2019)
- [48] Wang, H., Sridhar, S., Huang, J., Valentin, J., Song, S., Guibas, L.J.: Normalized object coordinate space for category-level 6d object pose and size estimation. In: Proceedings of the IEEE/CVF conference on computer vision and pattern recognition. pp. 2642–2651 (2019)
- [49] Wang, J., Karaev, N., Rupprecht, C., Novotny, D.: Vggsfm: Visual geometry grounded deep structure from motion. In: Proceedings of the IEEE/CVF conference on computer vision and pattern recognition. pp. 21686–21697 (2024)
- [50] Wang, P., Jung, H., Li, Y., Shen, S., Srikanth, R.P., Garattoni, L., Meier, S., Navab, N., Busam, B.: Phocal: A multi-modal dataset for category-level object pose estimation with photometrically challenging objects. In: Proceedings of the IEEE/CVF conference on computer vision and pattern recognition. pp. 21222–21231 (2022)
- [51] Wang, Z., Zhang, Z., Pang, T., Du, C., Zhao, H., Zhao, Z.: Orient anything: Learning robust object orientation estimation from rendering 3d models. arXiv preprint arXiv:2412.18605 (2024)
- [52] Wang, Z., Zhang, Z., Xu, J., Wang, J., Pang, T., Du, C., Zhao, H., Zhao, Z.: Orient anything v2: Unifying orientation and rotation understanding. arXiv preprint arXiv:2601.05573 (2026)
- [53] Wu, S., Li, R., Jakab, T., Rupprecht, C., Vedaldi, A.: Magicpony: Learning articulated 3d animals in the wild. In: Proceedings of the IEEE/CVF Conference on Computer Vision and Pattern Recognition. pp. 8792–8802 (2023)
- [54] Wu, X., Jiang, L., Wang, P.S., Liu, Z., Liu, X., Qiao, Y., Ouyang, W., He, T., Zhao, H.: Point transformer v3: Simpler faster stronger. In: Proceedings of the IEEE/CVF conference on computer vision and pattern recognition. pp. 4840–4851 (2024)
- [55] Xiang, Y., Kim, W., Chen, W., Ji, J., Choy, C., Su, H., Mottaghi, R., Guibas, L., Savarese, S.: Objectnet3d: A large scale database for 3d object recognition. In: European conference on computer vision. pp. 160–176. Springer (2016)
- [56] Xiang, Y., Mottaghi, R., Savarese, S.: Beyond pascal: A benchmark for 3d object detection in the wild. In: IEEE winter conference on applications of computer vision. pp. 75–82. IEEE (2014)
- [57] Xiao, Y., Du, Y., Marlet, R.: Posecontrast: Class-agnostic object viewpoint estimation in the wild with pose-aware contrastive learning. In: 2021 International Conference on 3D Vision (3DV). pp. 74–84. IEEE (2021)
- [58] Yang, L., Kang, B., Huang, Z., Zhao, Z., Xu, X., Feng, J., Zhao, H.: Depth anything v2. Advances in Neural Information Processing Systems **37**, 21875–21911 (2024)
- [59] Yu, X., Rao, Y., Wang, Z., Liu, Z., Lu, J., Zhou, J.: Pointr: Diverse point cloud completion with geometry-aware transformers. In: Proceedings of the IEEE/CVF international conference on computer vision. pp. 12498–12507 (2021)

- [60] Yue, Y., Robert, D., Wang, J., Hong, S., Wegner, J.D., Rupprecht, C., Schindler, K.: Litept: Lighter yet stronger point transformer. arXiv preprint arXiv:2512.13689 (2025)
- [61] Zhang, J., Lin, H., Hou, J., Xue, X., Fu, Y.: Beyond'templates': Category-agnostic object pose, size, and shape estimation from a single view. arXiv preprint arXiv:2510.11687 (2025)
- [62] Zhang, J., Huang, W., Peng, B., Wu, M., Hu, F., Chen, Z., Zhao, B., Dong, H.: Omni6dpose: A benchmark and model for universal 6d object pose estimation and tracking. In: European Conference on Computer Vision. pp. 199–216. Springer (2024)
- [63] Zhang, L., Wang, Z., Zhang, Q., Qiu, Q., Pang, A., Jiang, H., Yang, W., Xu, L., Yu, J.: Clay: A controllable large-scale generative model for creating high-quality 3d assets. ACM Transactions on Graphics (TOG) **43**(4), 1–20 (2024)
- [64] Zhang, Y., Zhang, L., Ma, R., Cao, N.: Texverse: A universe of 3d objects with high-resolution textures. arXiv preprint arXiv:2508.10868 (2025)
- [65] Zheng, L., Wang, C., Sun, Y., Dasgupta, E., Chen, H., Leonardis, A., Zhang, W., Chang, H.J.: Hs-pose: Hybrid scope feature extraction for category-level object pose estimation. In: Proceedings of the IEEE/CVF conference on computer vision and pattern recognition. pp. 17163–17173 (2023)
- [66] Zheng, Z., Yu, T., Dai, Q., Liu, Y.: Deep implicit templates for 3d shape representation. In: Proceedings of the IEEE/CVF conference on computer vision and pattern recognition. pp. 1429–1439 (2021)
- [67] Zhou, X., Karpur, A., Luo, L., Huang, Q.: Starmap for category-agnostic keypoint and viewpoint estimation. In: Proceedings of the European Conference on Computer Vision (ECCV). pp. 318–334 (2018)
- [68] Zhou, Y., Barnes, C., Lu, J., Yang, J., Li, H.: On the continuity of rotation representations in neural networks. In: Proceedings of the IEEE/CVF conference on computer vision and pattern recognition. pp. 5745–5753 (2019)

Supplementary Material

Every9D-21M: Large-Scale Canonicalized Real-World 9D Pose Estimation

This supplementary material provides additional details and results that complement the main paper. In Section S7, we present further ablations on the design choices that enabled our method to scale to more than 100K objects with limited computational resources. Further, in Section S8, we provide more details about the dataset and in Section S9 about the training. In Section S10, we describe how orientations are defined for all LVIS categories appearing in uCO3D [30]. In Section S11, we show our annotation and verification tools and quantify the human effort required to ensure a high-quality dataset. Finally, in Section S12, we provide additional qualitative examples of our canonicalized objects.

S7 Canonicalization Design Choices

In Table S5, we illustrate that CLIP features perform worse than DINOv3 features, likely because the contrastive objective separates semantically related categories (e.g., motorcycles and bicycles) despite their similar geometry. Furthermore, using 32 frames performs only 1.5 percentage points worse than using 64 frames, while substantially reducing computation. This efficiency enables our approach to scale to over 100K objects.

In Table S6, we quantify the verification process. Overall, 74.9% of videos are successfully annotated, while the remaining ones are mostly unsuitable for pose estimation due to poor reconstruction or the presence of multiple objects.

S8 Dataset details.

We provide the category distribution across super-categories in Figure S6.

For each of the 700 categories, we randomly sample five videos to form the test split, resulting in a balanced set of test videos. To obtain a computationally manageable yet diverse evaluation set, we uniformly sample 16 frames from each video. Each image is then cropped using the bounding box derived from its corresponding object mask.

All remaining videos are used for training. While evaluation is conducted on the 700 filtered categories, the training set retains coverage over all 905 categories. This filtering criterion guarantees that each evaluated category contains at least five training videos, avoiding degenerate regimes in the reported results.

Licenses and Terms of Use of External Assets

uCO3D is used in accordance with its official license terms. The dataset is released under the Creative Commons Attribution 4.0 International (CC BY 4.0) license, and we credit the original authors accordingly.

S9 Training Details.

We weight the translation, rotation, and object size loss with 1., 0.1, and 1..

We observed instability when training LitePT directly on the raw input point clouds. To mitigate this issue, we normalize each point cloud by subtracting the median and scaling using the interquartile range. Additionally, we clamp points beyond a predefined maximum distance in the normalized space.

We train our model for 100K iterations with a global batch size of 128. Training is conducted on 4 GPUs, where each batch is evenly distributed across devices. At the beginning of every epoch, we perform both inter-shard shuffling and intra-shard shuffling to ensure effective data randomization and reduce sampling bias.

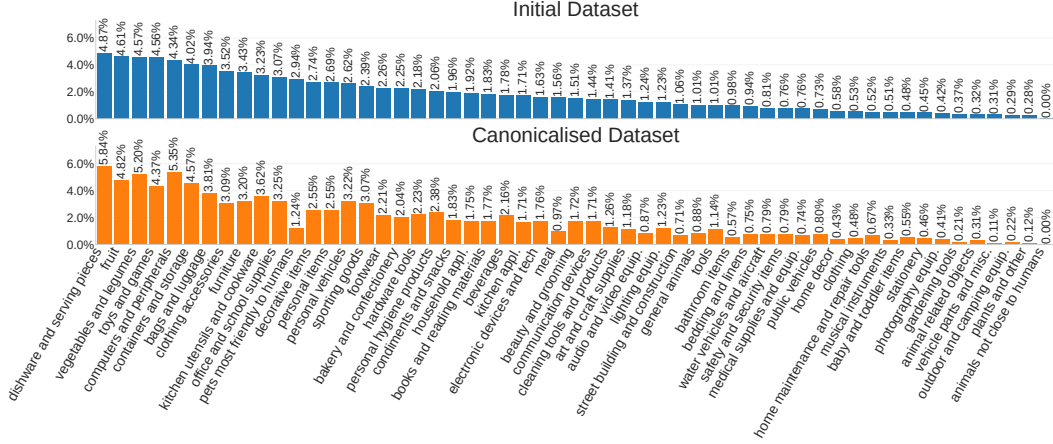


Figure S6: **Super-Category Distribution.** Every9D-21M covers a broad range of object categories. Our filtering process preserves the broad distribution.

Table S5: **Canonicalization Design Choices.** We evaluate key design decisions for clustering and automatic alignment on the annotated subset of CO3D [40, 14].

| Backbone | #Frames | Acc@30° |
|--------------|---------|---------|
| DINOv3-ViT-L | 32 | 82.2 |
| DINOv3-ViT-L | 64 | +1.5 |
| DINOv3-ViT-L | 16 | -2.7 |
| DINOv3-ViT-L | 4 | -3.4 |
| CLIP-ViT-L | 64 | -5.4 |

Following [61], we adopt the AdamW optimizer [31] with an initial learning rate of 1×10^{-4} and a weight decay of 5×10^{-4} . We employ an exponential learning rate scheduler with a decay factor of 0.98. Our model comprises 37M parameters, of which 15M are trainable.

S10 Orientations

We define three categories of directions: 22 intrinsic object directions, 16 extrinsic object–user directions, and 5 extrinsic object–user–object directions. Note that some relations correspond to axes rather than directed orientations due to underlying symmetries.

S10.1 Intrinsic directions.

"move backward": Opposite direction of natural forward movement, e.g. cow.

"move upward": Upward direction of movement or during movement, e.g. frisbee.

"move backward and forward": Axis of natural forward and backward movement, e.g. skateboard.

"contain or support upward": Direction upwards of supporting or containing other objects or liquids. e.g. bag.

"contain or support upward and downward": Direction upwards of supporting or containing other objects or liquids, e.g. hourglass.

Table S6: **Verification Statistics.**

| Iter. | Accept | Skipped | Filtered |
|-------|--------|---------|----------|
| 1st | 63.3% | 19.6% | 17.1% |
| 2nd | 59.0% | 35.8% | 5.2% |
| Total | 74.9% | 7.0% | 18.1% |

"cover upward": Direction of covering from falling objects or liquid, e.g. umbrella.

"cover upward and downward": Axis of covering from falling objects or liquid, e.g. blanket.

"entry backward": Opposite direction of entry, e.g. back of door.

"stand upward": Natural standing direction. Often defined via gravity.

"stand upward downward": Natural standing axis. Often defined via gravity.

"face backward": Backward of face for things with face that are not moving, e.g. teddy bears.

"sprout upward": Direction of sprout, e.g. onion.

"sprout upward and downward": Axis of sprout, when direction is unclear, e.g. log.

"stem upward": Stem direction of hanging fruits, e.g. apples.

"winding axis": Winding axis for e.g. tape.

"flow backward": Opposite of flow direction, flow may be arrows, liquid, wind, light, or electric signal.

"flow backward and forward": Axis of flow direction.

"unwinding extension backward": Opposite direction of unwinding.

"eyelet axis": Axis of eyelet, e.g. wristband, or, rubberband.

"toward mount backward": Backward horizontal mounting direction, e.g. sink.

"toward and away from mount backward": Mounting horizontal axis, e.g. deadbolt.

"toward mount upward": Upward vertical mounting direction, e.g. lightbulb.

S10.2 Extrinsic object-user directions.

"away from user": Direction that points away from user, e.g. faucet.

"away from user fingers": Direction that points away from user fingers, e.g. keyboard.

"toward and away from user": Axis that points towards and away from user, e.g. ironing board.

"user upward": Direction of user upward, e.g. raincoat.

"user backward": Direction of user backward, e.g. raincoat.

"user upward and downward": Axis of user upward and downward, e.g. headband.

"user lying axis head feet": Axis of user lying between head and feet, e.g. mattress.

"user forward and backward": Axis of user forward and backward, e.g. headset.

"along grab two hands left right": Axis of hands grabbing left and right, e.g. tray.

"along grab two hands away from function": Opposite of functional direction for tools required two hands, e.g. mop.

"along grab one hand": Axis for symmetric functional directions of tools grabbed with one hand, e.g. wrench.

"along grab one hand toward function": Functional direction for tools grabbed with one hand, e.g. hammer.

"along stand grab one hand grab away from function": Functional direction for tools which can stand, but also be grabbed with one hand, e.g. pan.

"along grab two fingers toward function": Functional direction for tools grabbed with two fingers, e.g. pencil.

"hand fingers": Direction of user's finger tip, e.g. glove.

"hand back": Direction of user's hand back, e.g. baseball glove or cup.

S10.3 Extrinsic object-user-object directions.

"away from object": Direction pointing away from another object, e.g. spoon.

"toward and away from object": Direction of point away and toward another object, e.g. racket.

"object upward": Direction of upward of another object, e.g. corkscrew.

"object squeeze": Axis of squeezing an object, e.g. scissor.

"object squeeze back": Direction toward the squeezing side that is moving more, whereas the other part is usually always in contact with the other object, e.g. barrette.

S10.4 Category-Level Mapping.

We provide category-level mappings to our defined orientations for 1067 LVIS categories that appear in uCO3D [30]. Note that we can reduce the 1067 categories to 95 orientation categories.

LEFT -, BACK user backward, TOP stand upward: bench, chair, sofa, slide, armchair, chaise longue, rocking chair, recliner, folding chair, loveseat, cabinet, sofa bed, deck chair, mouse computer equipment, vacuum cleaner, bedpan, highchair

LEFT -, BACK move backward, TOP move upward: airplane, dog, cart, lawn mower, kite, bicycle, tricycle, school bus, race car, cab taxi, jeep, convertible automobile, motorcycle, dirt bike, golfcart, pickup truck, bus vehicle, motor vehicle, car automobile, motor scooter, minivan, fire engine, giraffe, cock, ram animal, chicken animal, turtle, penguin, deer, hog, bird, mallard, owl, monkey, camel, cow, frog, horse, seahorse, crow, zebra, goat, duckling, goose, black sheep, domestic ass, elephant, sheep, giant panda, duck, flamingo, dove, gazelle, cub animal, polar bear, seabird, elk, bull, lamb animal, alligator, gorilla, crab animal, calf, parrot, foal, pony, dolphin, rabbit, bulldog, squirrel, puppy, shepherd dog, goldfish, kitten, parakeet, cat, dalmatian, hamster, ferret, pet, rodent, pug dog, handcart, grizzly, prawn, barrow, plow farm equipment, ferry, cruise ship, jet plane, cargo ship, boat, water scooter, passenger ship, blimp, helicopter, river boat, fighter jet, yacht, space shuttle, train railroad vehicle, garbage truck, trailer truck, truck, tractor farm equipment, police cruiser, bullet train, army tank, forklift, tow truck, bulldozer, ambulance, horse buggy, camper vehicle, wheelchair, baby buggy

LEFT -, BACK toward and away from user, TOP contain or support upward: handbag, suitcase, briefcase, envelope, box, mat gym equipment, wristlet, identity card, matchbox, shoulder bag, pouch, shopping bag, tote bag, cooler for food, duffel bag, ironing board

LEFT -, BACK away from user, TOP contain or support upward: backpack, palette, coloring material, pencil box, trash can, locker, bread bin, mailbox at home, perfume, shampoo, cigar box, saddlebag, clutch bag, wallet, satchel, cigarette case, hatbox, toolbox, dumpster, towel rack, water cooler

LEFT -, BACK away from user, TOP along grab one hand toward function: hair dryer, razorblade, hairbrush, shaver electric, toothbrush

LEFT -, BACK hand back, TOP hand fingers: baseball glove, boxing glove, potholder, mitten, glove

LEFT -, BACK toward and away from object, TOP along grab one hand toward function: tennis racket, racket, bottle opener, peeler tool for fruit and vegetables, spatula, file tool, scraper, hammer, mallet, sword, dagger

LEFT -, BACK -, TOP along grab one hand toward function: baseball bat, igniter, blender, crossbar, sparkler fireworks, eggbeater, skewer, cooking utensil, stirrer, masher, chap, boom microphone, microphone, flashlight, screwdriver, drumstick

LEFT -, BACK move backward and forward, TOP move upward: skateboard, canoe, raft, houseboat, drone, railcar part of a train, cabin car, freight car, wagon, passenger car part of a train

LEFT -, BACK -, TOP -: ball, cube, ping pong ball, volleyball, softball, soccer ball, seashell, gemstone, dishtowel, baseball, basketball, tennis ball, bowling ball, toy, jewel, jewelry, leather, die, beachball, medicine, musical instrument, sherbert, batter food, salsa, crouton, cast

LEFT -, BACK -, TOP along grab one hand: sausage, dumbbell, chocolate bar, string cheese, candy bar, egg roll

LEFT -, BACK -, TOP stand upward: sandwich, magnet, pad, paperweight, lightning rod, windsock, solar array, manhole, silo, water tower, streetlight, pole, baseball base, vase, candle holder, wreath, candle, flowerpot, pizza, cake, lego, checkerboard, gameboard, pool table, bun, brownie, cornbread, muffin, french toast, bread, pita bread, christmas tree, beanbag, dining table, footstool, coffee table, ottoman, table, kitchen table, stool, lamppost, lamp, oil lamp, lantern, birdbath, sail, cabana, tortilla, funnel, music stool, drum musical instrument, table lamp, chocolate cake, quiche, dish, casserole, battery, cone, doughnut, piggy bank, door, yurt, urn, ashtray, beef food, salmon food, hamburger, octopus food, steak food, bagel, turkey food, egg yolk, crabmeat, tripod, playpen, waffle, pretzel, crumb, truffle chocolate, toast food, pie, birthday cake, cookie, pancake, pastry, cupcake, eclair

LEFT -, BACK user backward, TOP user upward: camera, costume, raincoat, vest, overalls clothing, blazer, pajamas, suit clothing, bridal gown, trench coat, jean, corset, flannel, nightshirt, fleece, underwear, kilt, sportswear, sweater, parka, shirt, cardigan, jacket, tux, turtleneck clothing, ballet skirt, dress, coat, jersey, kimono, robe, lab coat, swimsuit, halter top, shoe, goggles, football helmet, rollerblade, helmet, choker, turban, legging clothing, suspenders, bow tie, cowboy hat, bandanna, spectacles, neckerchief, handkerchief, tiara, ice skate, roller skate, eyepatch, underdrawers, breechcloth, tartan, poncho, blinder for horses, bullhorn, camcorder, joystick, whistle, headscarf, baseball cap, bolo tie, lanyard, necklace, brassiere, tights clothing, shawl, sunglasses, crown, sock, visor, necktie, beret, apron, fedora, ski parka, cap headwear, cloak, gasmask, compass, crutch, cornet, saxophone, bagpipe, bass horn, clarinet, noseband for animals, nosebag for animals, armor, chain mail, mask, bulletproof vest, slipper footwear, boot, flip flop sandal, sandal type of shoe, ski boot, flipper footwear, arctic type of shoe, wooden leg, television camera, binoculars, bib

LEFT -, BACK -, TOP sprout upward: carrot, garlic, brussels sprouts, onion, cauliflower, asparagus, edible corn, ginger, green onion, tomato, green bean, legume, celery, turnip, mushroom, broccoli, radish, sweet potato, flower arrangement, carnation, bamboo, sunflower, bouquet, sugarcane plant, potato, artichoke, lettuce

LEFT -, BACK -, TOP stem upward: cucumber, pepper, eggplant, gourd, lime, grape, persimmon, clementine, mandarin orange, peach, blueberry, watermelon, date fruit, apple, pineapple, cantaloup, pear, blackberry, lemon, orange fruit, almond, pinecone, nut, raspberry, prune, coconut, apricot, avocado, papaya, kiwi fruit, fig fruit, strawberry, melon, cherry, bell pepper, pumpkin, chili vegetable, zucchini, chickpea

LEFT -, BACK away from user, TOP stand upward: parking meter, stop sign, fireplug, easel, sewing machine, shredder for paper, toaster, microwave oven, refrigerator, dishwasher, waffle iron, toaster oven, oven, coffee maker, mixer kitchen tool, food processor, stove, grill, postbox public, vending machine, telephone booth, elevator car, traffic light, street sign, newsstand, trunk, milestone, figurine, billboard, basketball backboard, window box for plants, subwoofer, cd player, radio receiver, amplifier, speaker stereo equipment, stereo sound system, record player, phonograph record, car battery, dollhouse, award, trophy cup, wardrobe, armoire, dresser, drawer, desk, cupboard, cash register, file cabinet, television set, laptop computer, piano, harmonium, microscope, globe, printer, router computer equipment, gargoyle, hookah, heater, radiator, fan, water heater, automatic washer, air conditioner, hotplate, generator, ice maker, first aid kit

LEFT along grab two hands left right, BACK toward and away from user, TOP contain or support upward: grocery bag, plastic bag

LEFT -, BACK -, TOP along grab two fingers toward function: needle, knitting needle, pencil, thumbtack, eraser, pen, marker, cigarette, stylus, bolt, crayon, sharpener, sharpie, pencil sharpener, dropper, syringe, lollipop

LEFT -, BACK -, TOP winding axis: bobbin, thread, cylinder, garden hose, toilet tissue, dental floss, tape sticky cloth or paper, hose, bandage, coil, tinfoil, paper towel, sushi, diaper

LEFT -, BACK toward and away from user, TOP along grab one hand toward function: paintbrush

LEFT -, BACK -, TOP hand fingers: thimble

LEFT -, BACK -, TOP eyelet axis: bead, wristband, bracelet, wedding ring, armband, anklet, rubber band, pipe, straw for drinking

LEFT -, BACK object squeeze, TOP along grab one hand toward function: pliers, shears, hair curler, nutcracker, tongs, scissors, curling iron

LEFT -, BACK away from object, TOP along grab one hand toward function: ax, handsaw, fork, power shovel, kettle, spoon, strainer, steak knife, wooden spoon, ladle, pitchfork, knife, shovel, pocketknife, soup spoon

LEFT -, BACK toward and away from user, TOP stand upward: step stool, ladder, manger, table tennis table, clock tower, futon, stepladder, crescent roll, baguet

LEFT -, BACK flow backward, TOP stand upward: reamer juicer, dish antenna, machine gun, fire extinguisher, cream pitcher, glass drink container, projector, webcam

LEFT -, BACK away from user, TOP user upward: calendar, clipboard, binder, scoreboard, painting, passport, tachometer, book, rearview mirror, cellular telephone, earphone, telephone, birthday card, receipt, booklet, paperback book, map, hardback book, diary, phonebook, comic book, postcard, bible, road map, mirror, clock, inkpad, notebook, checkbook, inhaler, control, pocket watch, timer, watch, remote control, calculator, ipod, beeper, alarm clock, water faucet, faucet

LEFT -, BACK object squeeze back, TOP along grab one hand toward function: stapler stapling machine, can opener, clippers for plants

LEFT -, BACK away from object, TOP stand upward: puncher, iron for clothing

LEFT -, BACK object squeeze, TOP along grab two fingers toward function: clip, hairpin, bobby pin, pin non jewelry, clothespin

LEFT -, BACK -, TOP contain or support upward: jar, barrel, beer bottle, garbage, milk can, thermos bottle, beer can, lemonade, orange juice, chocolate milk, alcohol, tequila, smoothie, soya milk, fruit juice, milk, liquor, vodka, wine bottle, pop soda, milkshake, cider, root beer, martini, hot sauce, cocoa beverage, pepper mill, colander, wineglass, bowl, watering can, toothpick, spice rack, shaving cream, toothpaste, gargle, lip balm, bottle, paper plate, flute glass, salad plate, vat, pottery, gift wrap, packet, tank storage vessel, water bottle, clothes hamper, bucket, canister, birdfeeder, cleansing agent, hand glass, detergent, dishwasher detergent, atomizer, hamper, can, carton, crate, water jug, chocolate mousse, grits, whipped cream, honey, yogurt, peanut butter, hummus, bubble gum, vinegar, cayenne spice, cornmeal, icecream, jam, tabasco sauce, fudge, olive oil, sour cream, soup, mint candy, cracker, jelly bean, condiment, applesauce, fishbowl, nest, aquarium, soup bowl, place mat, sugar bowl, saucer, saltshaker, shot glass, chinaware, dixie cup, wine bucket, shaker, plate, aerosol can, bathtub, coaster, platter, chalice, squid food, crisp potato chip, salad, lamb chop, ham, stew, meatball, patty food, lasagna, coleslaw, omelet, bean curd, mashed potato, rib food, pudding, pickle, gelatin, cistern

LEFT along grab two hands left right, BACK -, TOP contain or support upward: keg, wok, pot, basket, tray

LEFT -, BACK unwinding extension backward, TOP winding axis: tape measure, duct tape

LEFT -, BACK along stand grab one hand grab away from function, TOP stand upward: cappuccino, cooker, frying pan, pan for cooking, pan metal container, saucepan, cup, mug, dustpan, teacup

LEFT along grab two hands left right, BACK away from user, TOP stand upward: crock pot

LEFT -, BACK flow backward, TOP contain or support upward: teakettle, coffeepot, measuring cup, dispenser, gravy boat, pitcher vessel for liquid, freshener, teapot

LEFT -, BACK toward and away from user, TOP user upward: crucifix, saddle blanket, dollar, coin, money, cassette, videotape, penny coin, tag, business card, parchment, card, bookmark, notepad, keycard

LEFT -, BACK toward mount backward, TOP cover upward: awning

LEFT -, BACK move backward, TOP contain or support upward: shopping cart

LEFT -, BACK toward mount backward, TOP stand upward: windmill, fireplace, pinwheel

LEFT -, BACK -, TOP sprout upward and downward: log

LEFT -, BACK flow backward and forward, TOP stand upward: telephone pole, mast

LEFT -, BACK hand back, TOP along grab one hand: football american

LEFT -, BACK flow backward, TOP user upward: bow weapon

LEFT -, BACK user backward, TOP user upward and downward: belt, belt buckle, gag, pacifier

LEFT -, BACK -, TOP user upward: sunhat, beanie, sweatband, sombrero, cincture, ring, wig, hairnet, dress hat, skullcap, bonnet, shower cap, walking stick, hat, veil, tambourine, dog collar, life buoy, walking cane

LEFT -, BACK toward mount backward, TOP -: cufflink, bow decorative ribbons, wheel, brake light, motor, broach, blinker, steering wheel, headlight, taillight, reflector, wall socket, latch, doorknob, cleat for securing rope, hinge, propeller, knob, button

LEFT -, BACK face backward, TOP stand upward: snowman, scarecrow, teddy bear, puppet, doll, rag doll, weathervane, sculpture, mascot, statue sculpture

LEFT -, BACK -, TOP toward mount upward: tinsel, bell, tassel, pendulum, chandelier, lightbulb, fire alarm

LEFT -, BACK away from user, TOP along grab two fingers toward function: nailfile, thermometer

LEFT -, BACK toward and away from user, TOP along grab one hand: soap, ice pack, butter

LEFT along grab two hands left right, BACK -, TOP contain or support upward and downward: chopping board

LEFT -, BACK toward and away from object, TOP stand upward: grater

LEFT -, BACK user backward, TOP contain or support upward: pipe bowl, tobacco pipe, diving board

LEFT -, BACK -, TOP object upward: corkscrew, cork bottle plug, bottle cap

LEFT along grab two hands left right, BACK -, TOP -: rolling pin, barbell, cymbal

LEFT -, BACK -, TOP cover upward: umbrella, parasol, lampshade, runner carpet, doormat

LEFT -, BACK away from object, TOP along grab two hands away from function: golf club

LEFT -, BACK flow backward, TOP along grab one hand toward function: rifle, gun, pistol, water gun

LEFT -, BACK away from user, TOP stem upward: banana

LEFT -, BACK toward and away from user, TOP -: bedspread, quilt, towel, blanket, pillow, poker chip, cushion, tarp, dishrag, napkin, cover, bath towel, hand towel

LEFT -, BACK -, TOP contain or support upward and downward: mattress, hourglass, burrito, taco

LEFT -, BACK away from user fingers, TOP user upward: scale measuring instrument, typewriter, computer keyboard

LEFT -, BACK toward and away from user, TOP toward mount upward: coat hanger, padlock, chime, triangle musical instrument, tea bag, combination lock, curtain, shower curtain

LEFT -, BACK user forward and backward, TOP user upward: scarf, headset, sling bandage, heart

LEFT -, BACK object squeeze back, TOP along grab two fingers toward function: barrette, safety pin

LEFT -, BACK toward and away from user, TOP along grab two fingers toward function: plume, popsicle

LEFT -, BACK -, TOP user upward and downward: headband

LEFT -, BACK toward mount backward, TOP toward mount upward: earring, cornice, shower head

LEFT -, BACK -, TOP move upward: frisbee, balloon, starfish, buoy

LEFT -, BACK toward mount backward, TOP user upward: poster, wall clock, toilet, handle, knocker on a door, brass plaque, washbasin, kitchen sink, sink, urinal, thermostat

LEFT -, BACK user lying axis head feet, TOP stand upward: bunk bed, bed

LEFT -, BACK flow backward, TOP -: spotlight, projectile weapon, telephoto lens, flash, camera lens

LEFT -, BACK user lying axis head feet, TOP contain or support upward: hammock, sleeping bag

LEFT -, BACK away from object, TOP toward mount upward: bait, hook

LEFT -, BACK toward and away from object, TOP along grab one hand: oar, sponge, crowbar, wrench

LEFT -, BACK toward and away from object, TOP along grab two hands away from function: broom, mop

LEFT -, BACK away from object, TOP along grab one hand: scrubbing brush

LEFT -, BACK toward and away from object, TOP toward mount upward: clasp

LEFT -, BACK away from object, TOP user upward: drill

LEFT -, BACK toward mount backward, TOP user upward and downward: pegboard

LEFT -, BACK away from object, TOP along grab two fingers toward function: key, candy cane

LEFT -, BACK -, TOP along grab two hands away from function: spear

LEFT -, BACK away from user fingers, TOP stand upward: violin, guitar

LEFT -, BACK away from user, TOP toward mount upward: cowbell

LEFT -, BACK entry backward, TOP contain or support upward: birdhouse, birdcage

LEFT -, BACK entry backward, TOP stand upward: kennel

LEFT -, BACK user forward and backward, TOP contain or support upward: stirrup

LEFT -, BACK -, TOP toward and away from mount backward: deadbolt

LEFT -, BACK away from user, TOP -: earplug, band aid

LEFT along grab two hands left right, BACK -, TOP eyelet axis: handcuff

LEFT -, BACK user backward, TOP -: shield

LEFT along grab two hands left right, BACK -, TOP stand upward: griddle

LEFT -, BACK flow backward and forward, TOP toward mount upward: wind chime

LEFT -, BACK -, TOP stand upward downward: crawfish, boiled egg, egg, fish food, salmon fish

S11 Manual Labor

Despite manually annotating only 1K 9D object poses, we verify all oriented objects in the dataset. On average, each 9D pose annotation requires approximately 4 minutes, while verification of a pose takes around 2 seconds. This corresponds to about 67 hours of human effort for manual 9D pose annotation and 132 hours for large-scale pose verification. In total, the dataset curation required approximately 200 hours of human labor.

We illustrate the annotation interface in Figure S7 and the verification interface in Figure S8.

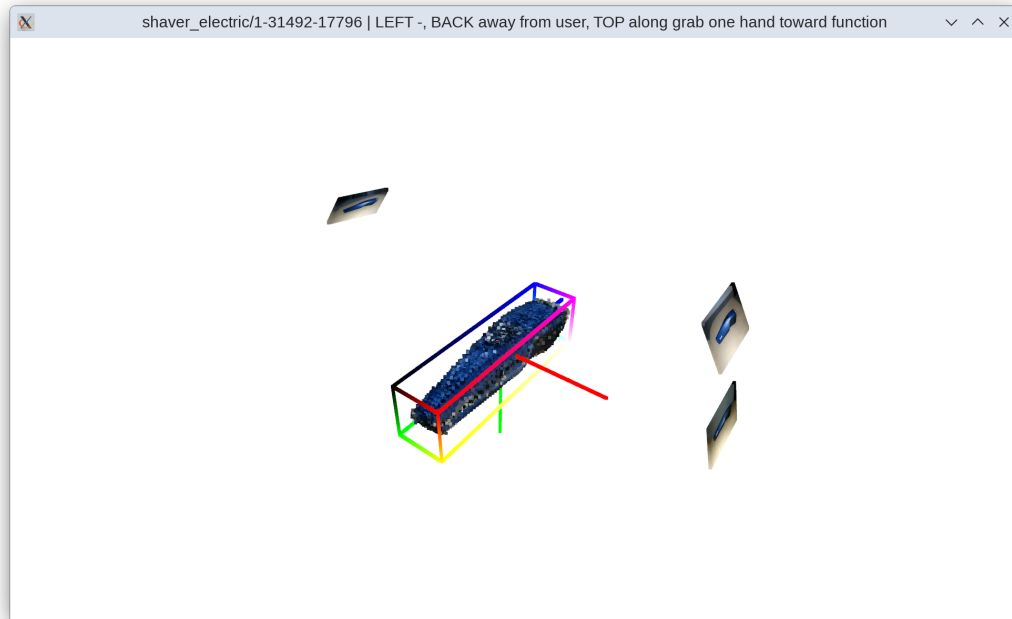


Figure S7: **Annotation Tool.** To annotate reference objects, we developed an interactive tool that enables precise 1° adjustments of the current axes while visualizing the oriented bounding box and canonical axes in real time. The tool also supports switching between different object views, which facilitates accurate refinement of the canonical frame.



Figure S8: **Verification Tool.** To verify objects, we render them from three views, front, top, and right. This enables us to discover fast and precise not aligned object instances and filter out objects due to bad reconstruction or multiple objects.

S12 Qualitative Examples

We provide a qualitative overview of 3D Gaussian Splatting reconstructions for a sample of 1,000 canonicalized objects spanning 200 categories. The examples illustrate the diversity of the dataset and the consistency of the resulting canonical object frames across instances and categories, see Figure S9.

S13 Societal Impact

Large-scale 9D pose estimation has the potential to advance applications in robotics, AR/VR, embodied AI, and 3D content creation by enabling systems to reason about object geometry, orientation, and physical interaction from visual observations. Improved object-centric spatial understanding may benefit assistive robotics, warehouse automation, autonomous manipulation, digital twin construction, and immersive virtual environments. Furthermore, scalable canonicalized real-world datasets can reduce reliance on synthetic data and support more robust and generalizable geometric foundation models.

At the same time, large-scale 9D pose estimation systems may introduce risks when deployed in real-world settings. Improved object tracking and scene understanding could contribute to surveillance applications or enable more capable autonomous systems in sensitive domains. Dataset biases, including imbalances in object categories, geographic distribution, or environmental conditions, may also lead to uneven performance across deployment settings. In addition, reliance on monocular depth estimation rather than sensor depth can propagate geometric inaccuracies, potentially affecting downstream safety-critical applications.

We mitigate some of these concerns by focusing on object-centric videos of everyday objects rather than human-centered data, and by releasing standardized evaluation protocols to encourage transparent benchmarking. Nevertheless, we emphasize that 9D pose foundation models should be deployed with appropriate safeguards, particularly in safety-critical or privacy-sensitive environments. Future work should further investigate fairness, robustness, uncertainty estimation, and mechanisms for preventing misuse in surveillance or autonomous decision-making systems.

Figure S9: Overview of Every9D-21M.



